Advances in Nano Research, *Vol. 16, No. 5 (2024) 445-458*
https://doi.org/10.12989/anr.2024.16.5.445

Static stability and vibration response of rotating carbon-nanotube-reinforced composite beams in thermal environment

Özge Özdemir*[1], Hüseyin Ural[1] and Alexandre de Macêdo Wahrhaftig[2]

[1]*Department of Aeronautical Engineering*, *Istanbul Technical University*, *34469*, *Maslak*, *Istanbul*, *Turkiye*
[2]*Department of Construction and Structures*, *Polytechnic School*, *Federal University of Bahia*, *BA*, *Brazil*

(*Received February 23, 2023, Revised March 20, 2024, Accepted April 1, 2024*)

Abstract. The objective of this paper is to present free vibration and static stability analyses of rotating composite beams reinforced with carbon nanotubes (CNTs) under uniform thermal loads. Beam structural equations and CNT-reinforced composite (CNTRC) beam formulations are derived based on Timoshenko beam theory (TBT). The temperature-dependent properties of the beam material, such as the elastic modulus, shear modulus, and material density, are assumed to vary over the thickness according to the rule of mixture. The beam material is modeled as a mixture of single-walled carbon nanotubes (SWCNTs) in an isotropic matrix. The SWCNTs are aligned and distributed in the isotropic matrix with different patterns of reinforcement, namely the UD (uniform), FG-O, FG-V, FG- Λ and FG-X distributions, where FG-V and FG-Λ are asymmetric patterns. Numerical examples are presented to illustrate the effects of several essential parameters, including the rotational speed, hub radius, effective material properties, slenderness ratio, boundary conditions, thermal force, and moments due to temperature variation. To the best of the authors' knowledge, this study represents the first attempt at the finite element modeling of rotating CNTRC Timoshenko beams under a thermal environment. The results are presented in tables and figures for both symmetric and asymmetric distribution patterns, and can be used as benchmarks for further validation.
Keywords: carbon-nanotube-reinforced composite beam; finite element method; stability analysis; thermal analysis; vibration analysis

1. Introduction

In many engineering systems, the design, material and dynamic properties of rotating components such as turbines, helicopter blades, and rotors have significant effects on the efficiency of the system. The dynamic behavior of carbon-nanotube-reinforced composites (CNTRCs) means that they have a wide range of applications, for example in wind turbine blades and the rotating blades of helicopters and light aircraft, and this represents a broad research topic.

Functionally graded carbon-nanotube-reinforced composite (FGCNTRC) beams have been shown to have superior mechanical and thermal properties of CNTs, and composite materials can be produced in the desired form and distribution with a 3D printer. The practical applications of CNT reinforcements in matrices of polymers or metals such as aluminum and magnesium, which are light materials, are becoming wide ranging. Several experimental, analytical and numerical studies of the mechanical and thermal properties of CNTRCs have been carried out. The disadvantages of conventional laminated composite materials, in which both the structure and properties change in a stepwise manner, include crack propagation and delamination; however, these disadvantages can be avoided by the use of functionally graded materials (FGMs) for structural components, where the material properties of the structure, such as the elastic modulus, shear modulus, Poisson's ratio, and material density, may change continuously in any desired direction as a function of the volume fraction and according to a simple power law.

Particularly for systems with variable speeds, the frequencies of the rotating structure and the rotor harmonics may intersect due to the changes in speed, thus inducing unsatisfactory vibrations in the structure. The use of compressive loads to alter the natural frequencies and avoid resonance is a well-known method. However, it is important to consider the magnitude of the compressive load to avoid buckling.

In this study, we investigate the bending vibration and buckling stability of functionally graded CNT-reinforced composite rotating beams subjected to thermal loads. To develop mathematical models and find solutions, the finite element method (FEM) is applied. The effects of several parameters are investigated, such as the rotational speed, hub radius, material properties, CNT distribution pattern, CNT volume fraction, temperature variation, boundary conditions, and slenderness ratio. The calculated results are compared with values in the literature, and very good agreement is observed.

It is worthing mention that as the novelty, the present work presents a finite element formulation for a rotating CNTRC Timoshenko beams under a thermal environment. To the best of the authors' knowledge, this study represents the first attempt at the finite element modeling in this sense. The results are presented in tables and figures for both symmetric and asymmetric distribution patterns, and can be used as benchmarks for further validations.

*Corresponding author, Associate Professor,
E-mail: ozdemirozg@itu.edu.tr

ISSN: 2287-237X (Print), 2287-2388 (Online)

2. Literature review

The literature contains a significant body of research on the mechanical behavior of CNTs and their usage in composites. For instance, the thermomechanical properties of nanocomposites made from epoxy and low weight fractions of randomly oriented single- and multi-walled CNTs were considered by Fadelus *et al*. (2005). The elastic properties of polymers reinforced with CNTs were investigated using molecular dynamic simulations by Han and Elliott (2007). Wuite and Adali (2005) found that the stiffness of CNTRC beams could be significantly improved by the homogeneous dispersion of a small percentage of CNTs. With the aim of defining the theoretical properties of SWCNTs, some elastic properties and effective wall thicknesses were studied by Wang and Zhang (2008). SWCNTs have also been modelled using spring-type finite elements of connected atoms to determine the effective mechanical properties (Giannopoulos *et al*. 2008, Lu and Hu, 2012). A higher-order energy-equivalent model was developed and the buckling behavior of SWCNTs was investigated by Mohamed *et al*. (2020). The forced response of SWCNT beams using doublet mechanics was studied by Eltaher *et al*. (2021), and it was suggested for the first time that the nonlinear bending behavior of CNTRC plates could be considerably improved through the use of a functionally graded distribution of CNTs in the matrix (Shen 2009). The forced vibration of higher-order functionally graded nanotubes was studied by Liu *et al*. (2022). Thermal bending and buckling, and the static, free and forced vibration behaviors of FGCNT graded plates and beams have also been investigated in the literature (Akurathi and Kolli 2017, Ansari *et al*. 2019, Di Sciuva and Sorrenti 2019, Feli *et al*. 2019, Fu *et al*. 2016, Karami *et al*. 2018, Khadir *et al*. 2021, Shen and Zhang 2010, Shen *et al*. 2019, Sobhy 2019, Torabi *et al*. 2019, Wu *et al*. 2019, 2020, Van Do *et al*. 2020, Vinyas 2019, Zhang *et al*. 2015, Zhou and Song, 2019, Zhu *et al*. 2012). Moreover, the energy harvesting of carbon-nanotube-reinforced beams has been studied by Mangalasseri *et al*. (2023). The acoustic responses of natural fiber-reinforced composite structures was considered by Satankar *et al*. (2020).

The linear and nonlinear dynamics of regular/FGM beams using FEM were studied by Chung and Yoo (2002) and Piovan and Sampaio (2009). Free vibration analyses of both rotating Euler-Bernoulli and Timoshenko FG beams, whose material properties change across the blade thickness, have also been studied through the use of the differential transform method (Özdemir 2016) and FEM (Demirsoy Karahan and Özdemir 2020). Moreover, the FE and Rayleigh methods (Rayleigh 1877) have been applied to analyze the free vibration and buckling stability of FGM Euler-Bernoulli and Timoshenko beams/columns of homogeneous elements and those where the material properties change in the spanwise direction (Kılıç and Özdemir 2021, Wahrhaftig and Magalhães 2021, Wahrhaftig *et al*. 2021).

The free vibration behavior of a FG rotating tapered beam with porosities was investigated by Tian *et al*. (2019). The nonlinear free vibration and modal interactions of rotating composite beams were studied by Arvin and Bakhtiari-Nejad (2013a, b) using TBT with the nonlinear von Karman strain displacement relationship and the Runge–Kutta method.

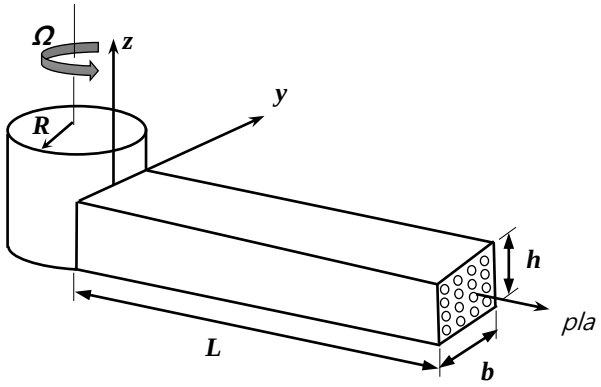

Fig. 1 Rotating FGCNTRC Timoshenko beam

With regard to rotating systems in a thermal environment, the dynamic behavior of a rotating micro FGM beam was investigated using a state-space representation of the motion equations (Bhattacharya and Das 2019). The response of a rotating hollow cylindrical FGM beam subjected to thermal loads was studied by Peng and Li (2010) using an analytical method based on the Fredholm integral equation. The rotational dynamics of a rotating FGCNTRC beam under thermal loads has been investigated using the generalized differential quadrature and differential transformation methods (Heidari and Arvin 2019, Khosravi *et al*. 2019a). A thermoelastic analysis of the axisymmetric bending of rotating disks of functionally graded material was also presented by Babamiri *et al*. (2020), where imperfection was considered.

As can be seen from the literature review, studies of the dynamic behavior and stability of rotating FGCNTRC beams subjected to thermal loads are limited. Only two works in this area have analyzed the subject analytically, and the parameters examined were limited to the temperature distribution, addition of CNTs and rotational speed.

3. FGCNTRC beams

In this study, we present a thermal vibration analysis of a rotating functionally graded beam made of SWCNT-reinforced matrix material (PMMA), as shown in Fig. 1. The axially oriented SWCNTs are distributed throughout the thickness, and the cross-sectional dimensions of the beam are kept constant in the spanwise direction.

Some different distribution patterns of CNTs in the thickness direction are shown in Fig. 2. Except for the uniform distribution (UD), each case (FG-V, FG-Λ, FG-O and FG-X) represents a functionally graded distribution.

The relation between the volume fractions of CNTs and the matrix material is obtained using the method of Shen and Xiang (2013), as follows:

$$V_{CNT} + V_m = 1 \tag{1}$$

Depending on the different CNT distribution patterns,

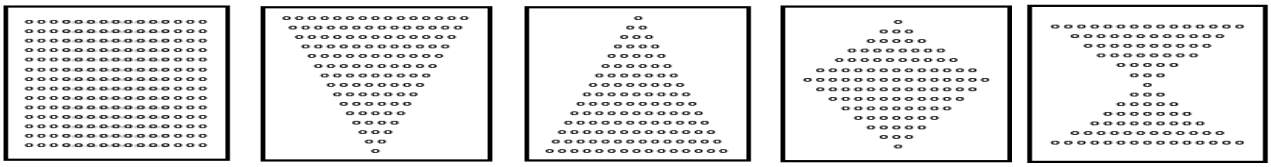

(a) (b) (c) (d) (e)

Fig. 2 Carbon nanotube distributions: (a) UD; (b) FG-V; (c) FG-Λ; (d) FG-O; (e) FG-X

Table 1 Efficiency constants η_i (Rahmani 2018)

Efficiency constants	V_{cnt}^*		
	0.12	0.17	0.28
η_1	0.137	0.142	0.141
η_2	1.022	1.626	1.585
η_3	0.7154	1.138	1.1095

the CNT volume fraction is calculated as follows (Wu *et al*. 2016, Zhu *et al*. 2012):

$$UD:\ V_{CNT} = V_{cnt}^* \tag{2}$$

$$FG-\Lambda:\ V_{CNT} = \left(1 - \frac{2z}{h}\right) V_{cnt}^* \tag{3}$$

$$FG-\mathrm{V}:\ V_{CNT} = \left(1 + \frac{2z}{h}\right) V_{cnt}^* \tag{4}$$

$$FG-\mathrm{O}:\ V_{CNT} = 2\left(1 - \frac{2|z|}{h}\right) V_{cnt}^* \tag{5}$$

$$FG-\mathrm{X}:\ V_{CNT} = \frac{4|z|}{h} V_{cnt}^* \tag{6}$$

where

$$V_{cnt}^* = \frac{W_{CNT}}{W_{CNT} + \frac{\rho_{CNT}}{\rho_m}(1 - W_{CNT})} \tag{7}$$

Since the material properties vary continuously along the *z*-axis, the effective properties of the nanocomposite are calculated using the rule of mixture model. Hence, the effective elastic and shear moduli of the CNTRC beam can be expressed as (Khosravi *et al*. 2019b):

$$E_{11} = \eta_1 V_{CNT} E_{11}^{CNT} + V_m E_m \tag{8}$$

$$\frac{\eta_2}{E_{22}} = \frac{V_{CNT}}{E_{22}^{CNT}} + \frac{V_m}{E_m} \tag{9}$$

$$\frac{\eta_3}{G_{12}} = \frac{V_{CNT}}{G_{12}^{CNT}} + \frac{V_m}{G_m} \tag{10}$$

Here, the symbols with $(\ )^{CNT}$ or $(\ )_{CNT}$ represent the parameters for CNTs, while $(\ )_m$ represents the parameters for the isotropic matrix material. The effective properties of the FGCNTRC beams are given as follows (Khosravi *et al*. 2019b):

$$\upsilon_{12} = V_{CNT}\upsilon_{12}^{CNT} + V_m\upsilon_m \tag{11}$$

$$\upsilon_{21} = \frac{\upsilon_{12}}{E_{11}} E_{22} \tag{12}$$

$$\rho = V_{CNT}\rho_{CNT} + V_m\rho_m \tag{13}$$

$$E = \frac{E_{11}}{1 - \upsilon_{12}\upsilon_{21}} \tag{14}$$

$$G = G_{12} \tag{15}$$

$$\alpha_{11} = \frac{V_{CNT}E_{11}^{CNT}\alpha_{CNT} + V_M E_M \alpha_M}{V_{CNT}E_{11}^{CNT} + V_M E_M} \tag{16}$$

For different values of V_{cnt}^*, the efficiency constants η_i have different values, as shown in Table 1.

4. Strain field for FGCNTRC rotating beams

Cross-sectional and longitudinal views of a Timoshenko beam undergoing an extension u_0 and flapwise bending deflections w are shown in Fig. 3. A reference point is chosen, and is represented as P_0 before deformation and P after deformation.

In Fig. 3, μ, ξ and x are the offsets of the reference point. The components of the strain tensor ε_{ij} are obtained as follows (Özdemir 2016):

$$\varepsilon_{xx} = u_0' + \frac{(u_0')^2}{2} + \frac{(w')^2}{2} + \varphi'\xi \tag{17}$$

$$\gamma_{x\mu} = 0 \tag{18}$$

$$\gamma_{x\xi} = w' + \varphi \tag{19}$$

where ε_{xx} is the axial strain, and $\gamma_{x\mu}$ and $\gamma_{x\xi}$ are the shear strains, respectively, where $(\ )'$ denotes differentiation with respect to the spanwise coordinate x.

5. Thermal environment and temperature distribution

CNTR beams have a wide area of engineering applicatio ns and because of the difference between the making tempe ratures and working temperatures of structures, for more eff icient design, it is important to take into account the thermal effects. Different temperature distribution patterns may be used as mentioned in open literature (Ghaffari *et al*. 2020)

5.1 Uniform temperature distribution (UTD)

For the case of UTD, the initial uniform temperature of the CNTR beam is assumed to be T_0, which refers to the ambient temperature and is a thermal strain free state. Under this temperature distribution pattern, the temperature

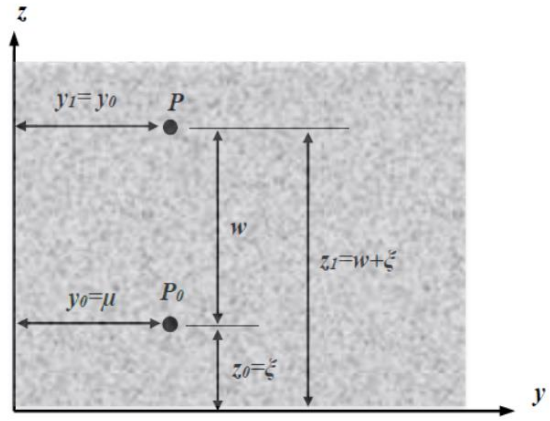

(a)

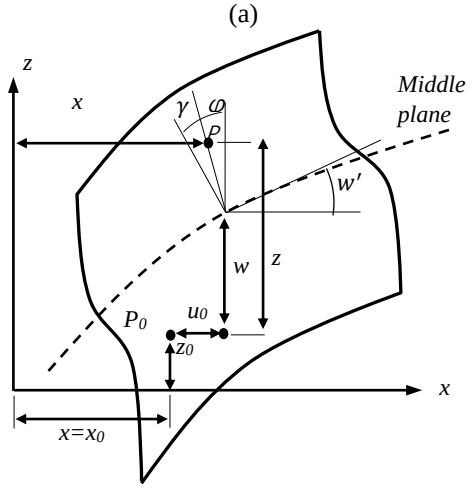

(b)

Fig. 3 (a) Cross-sectional view; (b) longitudinal view of the Timoshenko beam

of the CNTR beam is uniformly raised from T_0 to to the final temperature T with a difference ΔT as follows (Khosravi *et al*. 2019b):

$$\Delta T = T - T_0 \tag{20}$$

5.2 Linear temperature distribution (LTD)

For the linear temperature rise, the temperature of the bottom surface is T_b and the temperature is assumed to vary linearly along the thickness from T_b to T_t at the top surface. Thus, the temperature of a plane at a location z in the thickness direction (Kiani and Eslami 2013) is:

$$T(z) = T_b + (T_t - T_b)(\frac{h}{2} + \frac{z}{2}). \tag{21}$$

where h is the beam thickness and z is the vertical location of any point in the thickness direction.

5.3 Nonuniform temperature distribution (NLTD)

In the case of a nonuniform temperature rise, the temperature can be obtained by solving the following steady-state one-dimensional heat transfer equation with known temperature boundary conditions at the bottom and top surfaces of the beam (Zhang 2014). For the given boundary conditions and a variable thermal conductivity coefficient $\kappa(z)$, the temperature at a location z is:

$$\begin{aligned} &-\frac{d}{dz}\left(\kappa(z)\frac{dT}{dz}\right) = 0 \\ &T\left(\frac{h}{2}\right) = T_t, \quad T\left(-\frac{h}{2}\right) = T_b \\ &T(z) = T_b + \frac{T_t - T_b}{\int_{-\frac{h}{2}}^{\frac{h}{2}} \frac{1}{\kappa(z)} dz} \int_{-\frac{h}{2}}^{z} \frac{1}{\kappa(z)} dz \end{aligned} \tag{22}$$

5.4 Sinusoidal temperature distribution (STD)

The temperature field when the FG beam is exposed to a sinusoidal temperature rise across the thickness can be expressed as (Na and Kim 2004):

$$T = T_b + (T_t - T_b)\left[1 - Cos\frac{\pi}{2}\left(\frac{1}{2} + \frac{z}{h}\right)\right] \tag{23}$$

6. Energy expressions for FGCNTRC rotating beams in a thermal environment

In this study, a uniform temperature distribution is considered. We assume that the CNTR beam is at an initial temperature T_0 = 300 K and is stress free. Due to the temperature changes, thermal strain occurs, and is expressed as:

$$\varepsilon_T = \alpha_{11}(T - T_0) = \alpha_{11}\Delta T \tag{24}$$

where the temperature variation ΔT is assumed to be uniform in this study.

6.1 Potential energy

The expression for the potential energy of the beam is:

$$U = \frac{b}{2}\int_0^L \int_{-h/2}^{h/2} \{\sigma_{xx}(\varepsilon_{xx+}\varepsilon_T) + \tau_{x\xi}\gamma_{x\xi}\} d\xi \, dx \tag{25}$$

where (Khosravi *et al*. 2019a)

$$\sigma_{xx} = Q_{11}(\varepsilon_{xx+}\varepsilon_T) \tag{26}$$

$$\tau_{x\xi} = Q_{55}\gamma_{x\xi} \tag{27}$$

and

$$Q_{11} = \frac{E_{11}}{1 - \upsilon_{12}\upsilon_{21}} \tag{28}$$

$$Q_{55} = G_{12} \tag{29}$$

The mechanical axial force N_x, the mechanical bending moment M_x, and the shear force Q acting on a laminate at the midplane are expressed (Kollár and Springer 2003) as

follows. The thermal strain results in a thermal axial force N_T and a thermal bending moment M_T in addition to the mechanical ones (Yas and Samadi 2012):

$$(N_x, M_x) = b\int_{-h/2}^{h/2} Q_{11}\{1, (z-\bar{z}_0)\}dz \tag{30}$$

$$Q = b\int_{-h/2}^{h/2} Q_{55}dz \tag{31}$$

$$(N_T, M_T) = -b\int_{-h/2}^{h/2} Q_{11}\alpha_{11}\Delta T\{1, (z-\bar{z}_0)\}dz \tag{32}$$

where $\bar{z}_0$ is the physical neutral surface of the FGCNT reinforced beam (Ansari *et al*. 2014):

$$\bar{z}_0 = \frac{\int_{-h/2}^{h/2} Q_{11}z dz}{\int_{-h/2}^{h/2} Q_{11}dz} \tag{33}$$

By substituting Eqs. (30)-(33) into Eq. (25), the following expression can be obtained:

$$U = \frac{1}{2}\int_0^L \left\{N\left[u_0' + \frac{(w')^2}{2}\right] + M\varphi' + Q_{xz}(w'-\varphi)\right\} \tag{34}$$

where

$$N = A_{11}u_0' + B_{11}\varphi' + N_T \tag{35}$$

$$M = B_{11}u_0' + D_{11}\varphi' + M_T \tag{36}$$

$$Q = A_{55}\gamma_{x\xi} \tag{37}$$

The stiffness coefficients are obtained as follows (Khosravi *et al*. 2019a):

$$(A_{11}, B_{11}, D_{11}) = \int_{-h/2}^{h/2} Q_{11}\{1, (z-\bar{z}_0), (z-\bar{z}_0)^2\}dz \tag{38}$$

$$A_{55} = k\int_{-h/2}^{h/2} Q_{55}dz \tag{39}$$

The shear correction factor k has a value of $5/6$ or $\pi^2/12$ for rectangular cross-sections.

The uniform strain ε_0 and the associated axial displacement u_0 resulting from the centrifugal force $F_{CF}(x)$ are related to each other as follows (Özdemir Özgümüş and Kaya 2013):

$$u_0'(x) = \varepsilon_0(x) = \frac{F_{CF}(x)}{EA} = \frac{F_{CF}(x)}{A_{11}} \tag{40}$$

The expression for the centrifugal force is

$$F_{CF}(x) = \int_x^L \rho A\Omega^2(R+x)dx \tag{41}$$

Considering all the equations mentioned above, the final expression for the potential energy is:

$$U = \frac{1}{2}\int_0^L \{(D_{11}+M_T)(\varphi')^2 + A_{55}(w'-\varphi)^2 + (F_{CF}+N_T)(w')^2\}dx + C_1 \tag{42}$$

where C_1 is the integration constant.

As can be seen here, both the thermal axial force N_T and the centrifugal force F_{CF} are considered as external loads. When the carbon nanotube distribution is symmetric with respect to the midplane (i.e., UD, FG-O and FG-X), the thermal moment M_T becomes zero. However, in this study, nonuniform carbon nanotube distributions are also considered (i.e., FG-V and FG-Λ), and a nonzero M_T value will therefore be used in the formulation.

6.2 Kinetic energy

The position vector of point P in Fig. 3 is given by (Almitani 2019)

$$\vec{r_1} = (R + x + u_0 - \xi\varphi)\vec{\imath} + w\vec{k} \tag{43}$$

From Eq. (43), the velocity vector at this point is obtained as follows

$$\vec{V} = \frac{\partial\vec{r_1}}{\partial t} + \Omega\vec{k}\times\vec{r_1} = V_x\vec{\imath} + V_y\vec{\jmath} + V_z\vec{k} \tag{44}$$

Hence, the velocity components are

$$V_x = \dot{u}_0 - \xi\dot{\varphi} - \eta\Omega\ ,\quad V_y = (R + x + u_0 - \xi\varphi)\Omega,\ V_z = \dot{w} \tag{45}$$

The expression for the kinetic energy is

$$K = \frac{b}{2}\int_0^L\int_{-h/2}^{h/2}\rho(z)\left(V_x^2 + V_y^2 + V_z^2\right)d\xi\, dx + C_2 \tag{46}$$

where $\rho(z)$ is the effective material density given by Eq. (13) and C_2 is the integration constant.

Substituting the velocity components into Eq. (46) gives an expression for the kinetic energy as follows:

$$K = \int_0^L [I_1\dot{w}^2 + I_2(\dot{\varphi}^2 + \Omega^2\varphi^2)]dx + C_2 \tag{47}$$

where

$$(I_1, I_2) = \int_{-h/2}^{h/2}\rho(z)\{1, (z-\bar{z}_0)^2\}dz \tag{48}$$

7. Thermal analysis

The effect of a rise in temperature on the effective material properties is expressed as follows (Khosravi *et al*. 2019b):

$$\bar{P} = \overline{P_0} + \overline{P_1}(T/T_0) + \overline{P_2}(T/T_0)^2 + \overline{P_3}(T/T_0)^3 + \overline{P_4}(T/T_0)^4 \tag{49}$$

where $\overline{P_i}$ $(i = 0, \ldots, 4)$ are the coefficients of the interpolation function given in Table 2.

From Eq. (49) and the coefficients given in Table 2, the thermomechanical properties of SWCNT can be obtained at different temperatures as shown in Table 3.

In this study, polymethyl methacrylate (PMMA) is considered as a matrix material for the analysis. The variations in the mechanical properties of the PMMA matrix material are given in Table 4, where $\Delta T = T - T_0$ is the temperature variation, which is assumed to be uniform, and T_0 is the reference temperature of 300K.

Table 2 Coefficients of the interpolation function (Khosravi *et al*. 2019b)

Properties	Coefficients				
	$\overline{P_0}$	$\overline{P_1}$	$\overline{P_2}$	$\overline{P_3}$	$\overline{P_4}$
E_{11}^{CNT} (GPa)	6565.37	−1761.56	1133.47	−322.6	31.93
G_{12}^{CNT} (GPa)	1104.42	1884.27	−1476.23	490.29	−58.29
υ_{12}^{CNT}	−1.1280	6.8829	−2.60621	0.31023	−0.00054
α_{11}^{CNT} $(10^{-6}/K)$	0.175	0	0	0	0
ρ_{CNT} (kg/m^3)	1400	0	0	0	0

Table 3 Thermomechanical properties (Zhu *et al*. 2012)

T (K)	E_{11}^{CNT} (GPa)	G_{12}^{CNT} (GPa)	υ_{12}^{CNT}	α_{11}^{CNT} $(10^{-6}/K)$	ρ_{CNT} (kg/m^3)
300	5646.6	1944.5	0.175	3.4584	1400
400	5567.9	1970.3	0.175	4.1496	1400
500	5530.8	1964.3	0.175	4.5361	1400
700	5475.4	1964.4	0.175	4.6677	1400
1000	5281.4	1945.1	0.175	4.2800	1400

Table 4 Mechanical properties of the PMMA matrix material (Shen and Xiang 2013)

Mechanical properties	Expression/value
E_M, GPa	$3.52 - 0.0034T$
$\alpha_M, 10^{-6}/K$	$45 \times (1 + 0.0005 \times \Delta T)$
$\rho_M, kg/m^3$	1150
υ_M	0.34

Table 5 Efficiency constants η_i (Peng and Li 2010)

Efficiency constant	V_{cnt}^*		
	0.12	0.17	0.28
η_1	1.2833	1.3414	1.3238
$\eta_2 = \eta_3$	1.0556	1.7101	1.738

Table 6 Mechanical properties (Peng and Li 2010)

Mechanical property	Value	Mechanical property	Value
E_M, GPa	2.5	E_{22}^{CNT}, GPa	10
$\rho_M, kg/m^3$	1190	G_{12}^{CNT}, GPa	17.2
υ_M	0.3	ρ_{CNT}, kg/m^3	1400
E_{11}^{CNT}, GPa	600	υ_{12}^{CNT}	0.19

8. Finite element model

8.1 Displacement field and shape functions

The finite element model of the rotating beam is presented in this subsection. In Fig. 4, xyz is the global coordinate system, while $x'y'z'$ is the local coordinate system. The length of the element can vary along the beam

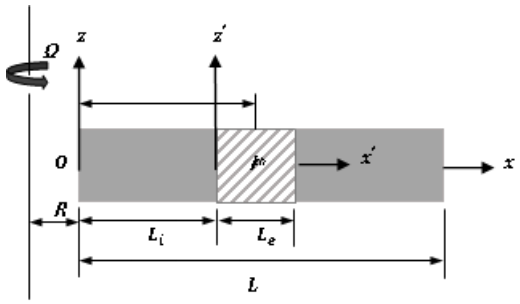

Fig. 4 Finite element model of a rotating beam

Fig. 5 Finite element model of the Timoshenko beam element

length, but in this study, the beam is divided into elements of equal length.

For a rotating beam, additional terms appear in the element matrices due to the centrifugal force. From Fig. 4, the centrifugal force given by Eq. (41) can be expressed as

$$F_{CF}(x) = \rho A\Omega^2[R(L - L_i - x') + \frac{1}{2}(L - L_i - x')(L - L_i + x')] \tag{50}$$

where

$$L_i = (i-1)\frac{L}{N_e} \tag{51}$$

Here, L is the length of the beam and N_e is the number of elements used in the finite element formulation. The finite element model of a Timoshenko beam element is shown in Fig. 5.

Here a two-node beam element with six degrees of freedom is considered, where the displacement field is defined according to the TBT.

Polynomials of appropriate order are defined for the displacement field as follows:

$$w = a_0 + a_1 x + a_2 x^2 + a_3 x^3 \tag{52}$$

$$\varphi = a_4 + a_5 x \tag{53}$$

$$\theta = w' - \varphi = a_1 - a_4 + (2a_2 - a_5)x + 3a_3 x^2 \tag{54}$$

Considering the displacement field polynomials, (Eqs. 52-54), the nodal displacements are determined as the displacement values at the first node of the element ($x = 0$) and at the second node ($x = L$), respectively. For the present beam model, the expressions for the displacements $\{q\}$, the nodal displacements $\{q_e\}$ are:

$$\{q\} = \{w \quad \theta \quad \varphi\}^T \tag{55}$$

$$\{q_e\} = \{w_1 \quad \theta_1 \quad \varphi_1 \quad w_2 \quad \theta_2 \quad \varphi_2\}^T \tag{56}$$

$$[N] = [N_w \quad N_\theta \quad N_\varphi]^T \tag{57}$$

where the matrices of the shape functions $[N]$ are given by

$$[N_w] = \left\{1 - \frac{3x^2}{{L_e}^2} + \frac{2x^3}{{L_e}^3} \quad x - \frac{2x^2}{L_e} + \frac{x^3}{{L_e}^2} \quad x - \frac{2x^2}{L_e} + \frac{x^3}{{L_e}^2} \quad \frac{3x^2}{{L_e}^2} - \frac{2x^3}{{L_e}^3} \quad -\frac{x^2}{L_e} + \frac{x^3}{{L_e}^2} \quad -\frac{x^2}{L_e} + \frac{x^3}{{L_e}^2}\right\} \tag{58}$$

$$[N_\theta] = \left\{-\frac{6x}{{L_e}^2} + \frac{6x^2}{{L_e}^3} \quad 1 - \frac{4x}{L_e} + \frac{3x^2}{{L_e}^2} \quad -\frac{3x}{L_e} + \frac{3x^2}{{L_e}^2} \quad \frac{6x}{{L_e}^2} - \frac{6x^2}{{L_e}^3} \quad -\frac{2x}{L_e} + \frac{3x^2}{{L_e}^2} \quad -\frac{3x}{L_e} + \frac{3x^2}{{L_e}^2}\right\} \tag{59}$$

$$[N_\varphi] = \left\{0 \quad 0 \quad 1 - \frac{x}{L_e} \quad 0 \quad 0 \quad \frac{x}{L_e}\right\} \tag{60}$$

8.2 Stiffness and mass matrices

From a consideration of the effect of centrifugal force and by substituting the shape functions into the potential and kinetic energy expressions in Eqs. (42) and (47), the element stiffness $[K^e]$ and element mass matrices $[M^e]$ are obtained for the Timoshenko beam model as:

$$[K^e] = \frac{1}{2}\int_0^L \left((D_{11} + M_T)\left[\frac{dN_\theta}{dx}\right]^T \left[\frac{dN_\theta}{dx}\right] + A_{55}\left(\left[\frac{dN_w}{dx}\right] - N_\theta\right)^T \left(\left[\frac{dN_w}{dx}\right] - N_\theta\right) + (F_{CF} + N_T)\left[\frac{dN_w}{dx}\right]^T \left[\frac{dN_w}{dx}\right]\right) dx \tag{61}$$

$$[M^e] = \frac{1}{2}\int_0^L (I_1[N_w]^T[N_w] + I_3[N_\theta]^T[N_\theta])\, dx \tag{62}$$

The components of the element stiffness are as follows:

$$[K^e]_f = \int_0^L (D_{11} + M_T)\left[\frac{dN_\theta}{dx}\right]^T \left[\frac{dN_\theta}{dx}\right] dx \tag{63}$$

$$[K^e]_s = \int_0^L A_{55}\left(\left[\frac{dN_w}{dx}\right] - N_\theta\right)^T \left(\left[\frac{dN_w}{dx}\right] - N_\theta\right) dx \tag{64}$$

$$[K^e]_g = \int_0^L (F_{CF} + N_T)\left[\frac{dN_w}{dx}\right]^T \left[\frac{dN_w}{dx}\right] dx \tag{65}$$

8.3 Modal and stability analyses

Depending on the number of elements used in the finite element model, the global matrices are obtained. After applying the boundary conditions, the reduced matrices are used for the following matrix equations:

$$[M]\{\ddot{q}\} + [K]\{q\} = \{0\} \tag{66}$$

where $[M]$ and $[K]$ are the reduced global mass and stiffness matrices, respectively (Arvin and Bakhtiari-Nejad 2013b).

The stiffness matrix is a combination of the flexural, shear and geometric stiffness matrices, as follows:

$$[K] = [K]_f + [K]_s + [K]_g \tag{67}$$

where $[K]_f$ is the global flexural stiffness matrix, $[K]_s$ is the global shear stiffness matrix, and $[K]_g$ is the global geometric stiffness matrix. Then, a modal analysis is applied to Eq. (67) to calculate the natural frequencies:

$$\left([K]_f + [K]_s + [K]_g - \omega^2[M]\right)\Phi = 0 \tag{68}$$

where Φ is the mode shape vector.

A buckling analysis is carried out by solving the following eigenvalue problem:

$$\left([K]_f + [K]_s - \lambda[K]_g\right)\Phi = 0 \tag{69}$$

where λ is the eigenvalue, $P_{cr} = -\lambda P$ is the critical buckling load, and P is the axial load, i.e., the negative centrifugal force $F_{CF}(x)$.

9. Results and discussion

In this subsection, the effects of several parameters (temperature changes, rotational speed, beam aspect ratio, hub radius, CNT amount and distribution, and different boundary conditions) are investigated and presented in several tables and figures. Validation against values in the literature is carried out where possible.

The mechanical and thermal properties of the CNTs at the reference temperature $T_0 = 300K$ are calculated and used in these analyses. The mechanical and thermal properties of the isotropic matrix material have already been given in Table 4.

The results are given in dimensionless form in the tables and figures. The dimensionless parameters are

$$\bar{\Omega} = \Omega\frac{L^2}{h}\sqrt{{\rho_M}/{E_M}} \qquad \bar{N}_{cr} = {N_{cr}}/{A_{10}}$$
$$\bar{\omega} = \omega L\sqrt{{I_{10}}/{A_{10}}} \qquad \delta = {R}/{L} \tag{70}$$

Here, $(A_{10}, I_{10}) = \int_{-h/2}^{h/2}(E_M,\ \rho_M)dz$, where E_M and ρ_M are the reference modulus of elasticity and the material density at T=300 K.

Case 1: Nonrotating FGCNTRC Timoshenko beam

In this subsection, the first five natural frequencies and the critical buckling load for a nonrotating FGCNTRC Timoshenko beam are calculated and compared with values given by Yas and Samadi (2012) and Wattanasakulpong and Ungbhakorn (2013). The effects of the boundary conditions, CNT volume fraction and distribution patterns on the natural frequencies and the critical buckling load are presented in Tables 7-10 for Ω = 0 rpm, L/h = 15, h = 0.01 m, and $\delta = 0$. The CNT efficiency constants used in the calculations are given in Table 5. The mechanical properties of both the matrix and CNT material are presented in Table 6.

From Tables 7-9, it can be observed that the CNT volume fraction V_{cnt} has an increasing effect on both the natural frequency and the buckling load. The FG-O distribution pattern of CNTs results in the lowest natural frequencies and buckling loads, while the FG-X distribution pattern gives the highest values.

Table 7 Natural frequency and buckling load versus V_{cnt} and CNT distribution patterns (hinged-hinged)

V_{cnt}	UD		FG-V		FG-X		FG-O	
	$\bar{\omega}$	$\bar{N}_{cr}$	$\bar{\omega}$	$\bar{N}_{cr}$	$\bar{\omega}$	$\bar{N}_{cr}$	$\bar{\omega}$	$\bar{N}_{cr}$
0.12	0.9896 *0.9976	0.1015 *0.1032 **0.098597	0.8552 *0.8592	0.0759 **0.09253	1.1366 *1.1485	0.1339 *0.1367 **0.128833	0.7599 *0.7628	0.0599 *0.0604 **0.058770
	2.9511	-	2.7074	-	3.1780	-	2.5057	-
	5.0356	-	4.7866	-	5.2550	-	4.5558	-
	7.0897	-	6.8691	-	7.2869	-	6.6471	-
0.17	1.2170	0.1549 **0.150559	1.0436	0.1140 **0.140748	1.4094	0.2077 **0.199945	0.9243	0.0894 **0.087704
	3.7194	-	3.3846	-	4.0448	-	3.1140	-
	6.4336	-	6.0823	-	6.7691	-	5.7568	-
	9.1222	-	8.8120	-	9.4394	-	8.4891	-
0.28	1.4655	0.2288 **0.220904	1.2730	0.1728 **0.209323	1.6862	0.3028 **0.289646	1.1340	0.1371 **0.133755
	4.2453	-	3.9565	-	4.6048	-	3.6774	-
	7.1368	-	6.9140	-	7.5380	-	6.6060	-
	9.9738	-	9.8579	-	10.4049	-	9.5678	-

*Wattanasakulpong and Ungbhakorn (2013), **Yas and Samadi (2012)

Table 8 Natural frequency and buckling load versus V_{cnt} and CNT distribution patterns (clamped-free)

V_{cnt}	UD		FG-V		FG-X		FG-O	
	$\bar{\omega}$	$\bar{N}_{cr}$	$\bar{\omega}$	$\bar{N}_{cr}$	$\bar{\omega}$	$\bar{N}_{cr}$	$\bar{\omega}$	$\bar{N}_{cr}$
0.12	0.3804 **0.3764	0.03358 **0.031234	0.3222 **0.3193	0.0223 **0.021985	0.4483 **0.4416	0.0453 **0.044355	0.2828 **0.2809	0.0170 **0.016790
	1.7500 **1.7006	-	1.5858 **1.5473	-	1.9118 **1.8497	-	1.4567 **1.4266	-
	3.7976 **3.6648	-	3.5518 **3.4380	-	4.0298 **3.8777	-	3.3466 **3.2489	-
	5.8716	-	5.6212	-	6.0983	-	5.3956	-
0.17	0.4638 **0.4587	0.0471 **0.046318	0.3903 **0.3866	0.0327 **0.032234	0.5498 **0.5413	0.0679 **0.066253	0.3420 **0.3394	0.0249 **0.024572
	2.1946 **2.1365	-	1.9732 **1.9287	-	2.4185 **2.3437	-	1.8029 **1.7685	-
	4.8210 **4.6614	-	4.4846 **4.3500	-	5.1560 **4.9706	-	4.2049 **4.0913	-
	7.5217	-	7.1740	-	7.8678	-	6.8562	-
0.28	0.5696 **0.5612	0.0740 **0.072178	0.4824 **0.4761	0.0516 **0.050475	0.6720 **0.6586	0.0953 **0.102480	0.4241 **0.4197	0.0394 **0.038680
	2.5332 **2.4614	-	2.3258 **2.2685	-	2.7864 **2.6987	-	2.1448 **2.0993	-
	5.4231 **5.2446	-	5.1555 **5.0007	-	5.8153 **5.6150	-	4.8741 **4.7399	-
	8.3010	-	8.0973	-	8.7377	-	7.7957	-

**Yas and Samadi (2012)

Case 2: Nonrotating FGCNTRC Timoshenko beam with variable slenderness ratio

In this case, the first three natural frequencies and the critical buckling load of a nonrotating FGCNTRC Timoshenko beam are calculated for different values of the slenderness ratio, L/h = 5, 10. The results for four different CNT distribution patterns (UD, FG-X, FG-O and FG-V) are given in Tables 10–12 for different boundary conditions and values of V_{cnt} = 0.12, 0.17 and 0.28. Here, Ω = 0 rpm, h = 0.01 m, $\delta = 0$, T = 300 K.

From Tables 10-12, it can be seen that as L/h increases, the natural frequencies and the critical buckling load become

Table 9 Natural frequency and buckling load versus V_{cnt} and CNT distribution patterns (clamped-clamped)

V_{cnt}	UD		FG-V		FG-X		FG-O	
	$\bar{\omega}$	$\bar{N}_{cr}$	$\bar{\omega}$	$\bar{N}_{cr}$	$\bar{\omega}$	$\bar{N}_{cr}$	$\bar{\omega}$	$\bar{N}_{cr}$
0.12	1.5626 **1.5085	0.2258 **0.213958	1.4507 **1.4068	0.1905 **0.181823	1.6647 **1.6000	0.2616 **0.245934	1.3538 **1.3180	0.1632 **0.156758
	3.2747 **3.1353	-	3.1234 **2.9997	-	3.4163 **3.2629	-	2.9856 **2.8762	-
	5.2352 **4.9979	-	5.0552 **4.8363	-	5.4044 **5.1514	-	4.8858 **4.6840	-
	7.2352	-	7.0581	-	7.4041	-	6.8802	-
0.17	1.9782 **1.9144	0.3620 **0.344251	1.8230 **1.7721	0.3006 **0.287861	2.1276 **2.0498	0.4276 **0.403501	1.6908 **1.6500	0.2544 **0.245191
	4.1878 **4.0187	-	3.9786 **3.8312	-	4.3995 **4.2111	-	3.7849 **3.6565	-
	6.7260 **6.4348	-	6.4794 **6.2139	-	6.9881 **6.6753	-	6.2391 **5.9970	-
	9.3315	-	9.0911	-	9.6056	-	8.8338	-
0.28	2.2365 **2.1618	0.4800 **0.455602	1.9795 **2.0504	0.3610 **0.346965	2.4035 **2.3169	0.5643 **0.532998	2.1121 **1.9284	0.4179 **0.399275
	4.6387 **4.4556	-	4.3203 **4.3414	-	4.9034 **4.7051	-	4.5051 **4.1740	-
	7.3791 **7.0745	-	7.0355 **6.9783	-	7.7298 **7.4093	-	7.2612 **6.7728	-
	10.1558	-	9.8701	-	10.5603	-	10.1037	-

**Yas and Samadi (2012)

Table 10 Natural frequency and buckling load versus Vcnt and *L*/*h* (hinged-hinged)

L/h	V_{cnt}	UD		FG-V		FG-X		FG-O	
		$\bar{\omega}$	$\bar{N}_{cr}$	$\bar{\omega}$	$\bar{N}_{cr}$	$\bar{\omega}$	$\bar{N}_{cr}$	$\bar{\omega}$	$\bar{N}_{cr}$
5	0.12	1.6785	0.2920	1.5955	0.2645	1.7517	0.3178	1.5186	0.2397
		3.7003		3.6479		3.7546		3.5871	
		5.6645		5.6350		5.7110		5.5900	
	0.17	2.1445	0.4811	2.0274	0.4312	2.2564	0.5320	0.8552	0.3865
		4.7909		4.7227		4.8864		2.7074	
		7.3575		7.3317		7.4498		4.7866	
	0.28	2.3789	0.6026	2.3047	0.5667	2.5127	0.6718	2.2020	0.5176
		5.1726		5.2036		5.3411		5.1258	
		7.8932		8.0124		8.1097		7.9555	
10	0.12	1.2855	0.1714	0.8552	0.1369	1.4226	0.2097	1.0419	0.1128
		3.3571		2.7074		3.5033		3.0372	
		5.4018		4.7866		5.5264		5.1240	
	0.17	1.6027	0.2688	1.4186	0.2111	0.8552	0.3355	0.8552	0.1721
		4.2891		4.0548		2.7074		2.7074	
		6.9659		6.7768		4.7866		4.7866	
	0.28	1.8726	0.3736	1.6917	0.3055	2.0808	0.4611	1.5415	0.2536
		4.7579		4.6093		5.0253		4.4040	
		7.5820		7.5411		7.8803		7.3571	

lower for all beam models. The boundary conditions also have a strong impact on the calculated values. The natural frequencies and the critical buckling loads become higher for beams with CF, HH and CC end conditions, respectively. The FG-X distribution pattern gives the largest natural frequency and critical load values, while the FG-O

Table 11 Natural frequency and buckling load versus V_{cnt} and L/h (clamped-free)

L/h	V_{cnt}	UD		FG-V		FG-X		FG-O	
		$\bar{\omega}$	$\bar{N}_{cr}$	$\bar{\omega}$	$\bar{N}_{cr}$	$\bar{\omega}$	$\bar{N}_{cr}$	$\bar{\omega}$	$\bar{N}_{cr}$
5	0.12	0.7660	0.1714	0.7073	0.1369	0.8194	0.2097	0.6574	0.1128
		2.4521		2.3462		2.5560		2.2670	
		4.5949		4.5205		4.6698		4.4492	
	0.17	0.9679	0.2688	0.8865	0.2111	1.0457	0.3355	0.8189	0.1721
		3.1402		3.0011		3.2915		2.8951	
		5.9461		5.8505		6.0733		5.7468	
	0.28	1.0986	0.3736	1.0315	0.3055	1.1845	0.4611	0.9631	0.2536
		3.4709		3.3771		3.6696		3.2670	
		6.4276		6.4509		6.6473		6.3578	
10	0.12	0.5236	0.0646	0.4539	0.0467	0.5990	0.0889	0.4040	0.0362
		2.0513		1.9150		2.1855		1.8048	
		4.2045		4.0294		4.3660		3.8752	
	0.17	0.6448	0.0972	0.5545	0.0694	0.7441	0.1354	0.4918	0.0534
		2.6020		2.4177		2.7906		2.2677	
		5.3878		5.1472		5.6328		4.9316	
	0.28	0.7741	0.1483	0.6750	0.1074	0.8870	0.2045	0.6025	0.0834
		2.9335		2.7804		3.1613		2.6287	
		5.9430		5.8016		6.2561		5.5941	

Table 12 Natural frequency and buckling load versus V_{cnt} and L/h (clamped-clamped)

L/h	V_{cnt}	UD		FG-V		FG-X		FG-O	
		$\bar{\omega}$	$\bar{N}_{cr}$	$\bar{\omega}$	$\bar{N}_{cr}$	$\bar{\omega}$	$\bar{N}_{cr}$	$\bar{\omega}$	$\bar{N}_{cr}$
5	0.12	1.9019	0.3648	1.8794	0.3544	1.8601	0.3448	1.8357	0.3336
		3.7904		3.7436		3.7043		3.6608	
		5.7601		5.7172		5.6935		5.6554	
	0.17	2.4777	0.6232	2.4366	0.5994	2.4133	0.5833	2.3764	0.5613
		4.9365		4.8531		4.8079		4.7450	
		7.5156		7.4287		7.4127		7.3551	
	0.28	2.7036	0.7585	2.6238	0.7116	2.6497	0.7208	2.6186	0.6997
		5.3895		5.2272		5.2762		5.2192	
		8.1778		7.9638		8.0923		8.0438	
10	0.12	1.8005	0.3178	1.7386	0.2920	1.6689	0.2645	1.6008	0.2397
		3.6073		3.5108		3.4136		3.3219	
		5.6037		5.5001		5.3970		5.2900	
	0.17	2.3259	0.3865	2.2291	0.4811	2.1308	0.5320	2.0332	0.4312
		4.6719		4.5217		4.3921		4.2615	
		7.2816		7.1086		6.9732		6.8179	
	0.28	2.5767	0.6718	2.4549	0.6026	2.4028	0.5667	2.3129	0.5176
		5.1532		4.9366		4.8910		4.7688	
		7.9821		7.7035		7.7101		7.5698	

distribution pattern gives the lowest.

Case 3: Rotating FGCNTRC Timoshenko beam

In this section, the variation in the fundamental frequency and the critical buckling load of a rotating FGCNTRC Timoshenko beam with the rotational speed and the hub radius are analyzed. The results are given in Figs. 6 and 7 for the CF boundary condition with values of V_{cnt} = 0.17 at T = 400 K and slenderness ratio L/h = 10. The

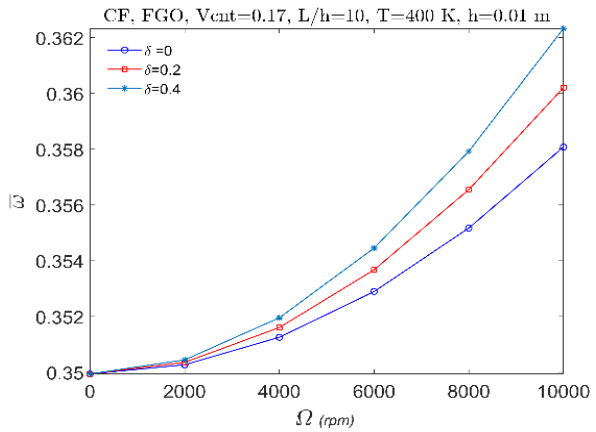

Fig. 6 Variation in the fundamental frequency of a rotating CNTRC CF-beam

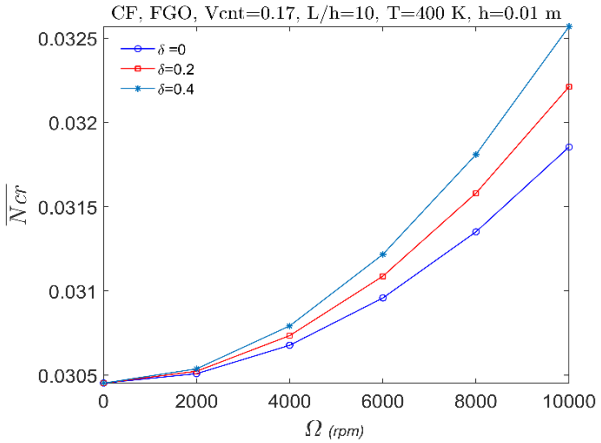

Fig. 7 Variation in the critical buckling load of a rotating CNTRC CF-beam

Table 13 Natural frequency and buckling load versus V_{cnt} and temperature (hinged-hinged)

	Ω = 10000 rpm					
T (K)	V_{cnt} = 0.12		V_{cnt} = 0.17		V_{cnt} = 0.28	
	$\bar{\omega}$	$\bar{N}_{cr}$	$\bar{\omega}$	$\bar{N}_{cr}$	$\bar{\omega}$	$\bar{N}_{cr}$
	1.0637	0.1180	1.3141	0.1821	1.5319	0.2529
300	2.7565		3.4981		3.8806	
	4.4256		5.6723		6.1793	
	1.0094	0.1140	1.25149	0.177172	1.4475	0.2423
350	2.6264		3.3439		3.68362	
	4.2127		5.41507		5.86224	
	0.9464	0.1081	1.17912	0.1696	1.3487	0.226839
400	2.4803		3.17146		3.4606	
	3.9762		5.13067		5.5069	
	0.8745	0.1001	1.09681	0.159263	1.23485	0.2064
450	2.3180		2.98047		3.21079	
	3.7159		4.81876		5.11226	
	0.7928	0.0900	1.00378	0.1458	1.1038	0.180239
500	2.1383		2.76977		2.9318	
	3.4302		4.4778		4.6753	

mechanical and thermal properties given in Tables 1-4 are used in this case.

It can be seen that the natural frequencies and the critical buckling load increase with the rotational speed; this is due to the stiffening effect of the centrifugal force, which is proportional to the square of the rotational speed. Moreover, the rate of increment becomes larger with the hub radius parameter δ, as the centrifugal force is also directly proportional to the hub radius.

Case 4: Rotating FGCNTRC Timoshenko beam under thermal effect

In this case. the first three natural frequencies and the critical buckling load of the FGCNTRC Timoshenko beams with HH boundary conditions are given in Table 15 for rotating condition. The results are calculated for the FG-V distribution pattern with values of V_{cnt} = 0.12, 0.17 and 0.28 at L/h = 10, h = 0.01 m, $\delta = 0$. The mechanical and thermal properties given in Tables 1–4 are used in this case.

From Table 15, it can be observed that a temperature increase has a decreasing effect on the natural frequencies and the critical buckling load; this is due to the softening effect.

10. Conclusions

The dynamic behavior and stability of rotating composite beams reinforced with CNTs has been investigated. The effects of the rotational speed, temperature change, the amount and distribution of CNTs, the hub radius, and the beam aspect ratios have been examined for different boundary conditions. Based on the tables and figures presented here, the following comments can be made:

• The CNT volume fraction V_{cnt} has an increasing effect on the natural frequency and the critical buckling load, as an increase in the fraction of carbon nanotubes in the matrix material makes the beam stiffer (Karamanlı and Vo 2021).

• The slenderness ratio L/h has a decreasing effect on the natural frequency and the critical buckling load, since as the beam gets more slender, buckling becomes easier.

• The FG-X CNT distribution pattern gives the largest values for the natural frequency and the critical buckling load, followed by the UD, FG-Λ, and FG-O patterns. It is clear that the presence of CNTs in the inner and outer surfaces has more effect than at the mid-span. This indicates that the use of CNTs alone to reinforce the pipes is not sufficient, and the distribution of CNTs should also be considered when producing pipes (Ghasemi and Soleymani, 2021).

• The natural frequencies and the critical buckling loads are higher for beams with the CC, HH and CF end conditions, respectively; this is because the effective length of the beam becomes larger from the CC to CF boundary conditions, making buckling easier.

• The natural frequency increases with the rotational speed, and the rate of increment becomes larger with the hub radius parameter δ, while the temperature increase has a decreasing effect on the natural frequency and the critical buckling load due to the softening effect.

References

Akurathi, V.L. and Kolli, L.C. (2017), "Free vibration behavior of FG-CNT reinforced composite plates using higher order shear deformation theory", *Int. J. Res. Appl. Sci. Eng. Technol.*, **5**(11), 1408-1418. https://doi.org/10.22214/ijraset.2017.11204

Almitani, K.H. (2019), "On forced and free vibrations of cutout squared beams", *Steel Compos. Struct.* **32**(5), 643-655. https://doi.org/10.12989/scs.2019.32.5.643

Ansari, R., Torabi, J. and Hassani, R. (2019), "Thermal buckling analysis of temperature-dependent FG-CNTRC quadrilateral plates", *Comput. Math. Appl.* **77**(5), 1294-1311. https://doi.org/10.1016/j.camwa.2018.11.009

Ansari, R., Faghih Shojaei, M., Mohammadi, V., Gholami, R. and Sadeghi, F. (2014), "Nonlinear forced vibration analysis of functionally graded carbon nanotube-reinforced composite Timoshenko beams", *Compos. Struct.*, **113**(1), 316-327. https://doi.org/10.1016/j.compstruct.2014.03.015

Arvin, H. and Bakhtiari-Nejad, F. (2013a), "Nonlinear free vibration analysis of rotating composite Timoshenko beams", *Compos. Struct.*, **96**, 29-43. https://doi.org/10.1016/j.compstruct.2012.09.009

Arvin, H. and Bakhtiari-Nejad, F. (2013b), "Nonlinear modal interaction in rotating composite Timoshenko beams", *Compos. Struct.*, **96**, 121-134. https://doi.org/10.1016/j.compstruct.2012.10.015

Babamiri, B.B., Shahrjerdi, A. and Bayat, M. (2020), "Effect of geometrical imperfection on the thermomechanical behavior of functionally graded material rotating disk", *J. Braz. Soc. Mech. Sci. Eng.*, **42**, 271. https://doi.org/10.1007/s40430-020-02360-z

Bhattacharya, S. and Das, D. (2019), "Free vibration analysis of bidirectional-functionally graded and double-tapered rotating micro-beam in thermal environment using modified couple stress theory", *Compos. Struct.* **215**, 471-492. https://doi.org/10.1016/j.compstruct.2019.01.080

Chung, J. and Yoo, H.H. (2002), "Dynamic analysis of a rotating cantilever beam by using the finite element method", *J. Sound Vib.*, **249**(1), 147-164. https://doi.org/10.1006/jsvi.2001.3856

Demirsoy Karahan, E. and Özdemir, Ö. (2020), "Finite element formulation and free vibration analyses of rotating functionally graded blades", *J. Theor. Appl. Mech.*, **59**(1), 3-15. https://doi.org/10.1016/j.camwa.2018.11.009

Di Sciuva, M. and Sorrenti, M. (2019), "Bending, free vibration and buckling of functionally graded carbon nanotube-reinforced sandwich plates, using the extended Refined Zigzag Theory", *Compos. Struct.*, **227**, 111324. https://doi.org/10.1016/j.compstruct.2019.111324

Eltaher, M.A., Abdelrahman, A.A. and Esen, I. (2021), "Dynamic analysis of nanoscale Timoshenko CNTs based on doublet mechanics under moving load", *Eur. Phys. J. Plus* **123**, 1-21. https://doi.org/10.1140/epjp/s13360-021-01682-8

Eltaher, M.A. and Mohamed, S.A. (2020), "Buckling and stability analysis of sandwich beams subjected to varying axial loads", *Steel Compos. Struct.*, **34(**2), 241-260. https://doi.org/10.12989/scs.2020.34.2.241

Fadelus, J.D., Wiesel, E., Gojny, F.H., Schulte, K. and Wagner, H.D. (2005), "Thermo-mechanical properties of randomly oriented carbon/epoxy nanocomposites", *Compos. Part A,* **36**, 1555-1561. https://doi.org/10.1016/j.compositesa.2005.02.006

Feli, S., Karami, L. and Jafari, S.S. (2019), "Analytical modeling of low velocity impact on carbon nanotube-reinforced composite (CNTRC) plates", *Mech. Adv. Mater. Struct.* **26**(5), 394-406. https://doi.org/10.1080/15376494.2017.1400613

Fu, Y., Zhong, J., Shao, X. and Tao, C. (2016), "Analysis of nonlinear dynamic stability for carbon nanotube-reinforced composite plates resting on elastic foundations", *Mech. Adv. Mater. Struct.*, **23**(11), 1284-1289. https://doi.org/10.1080/15376494.2015.1068404

Ghaffari, S.S., Ceballes, S. and Abdelkefi, A. (2020), "Nonlinear dynamical responses of forced carbon nanotube-based mass sensors under the influence of thermal loadings", *Nonlinear Dyn* **100**, 1013–1035. https://doi.org/10.1007/s11071-020-05565-y

Ghasemi, A.R. and Soleymani, M. (2021), "Effects of carbon nanotubes distribution on the buckling of carbon nanotubes/ fiber/polymer/metal hybrid laminates cylindrical shell", *J. Sandw. Struct. Mater.* **23**(6), 2086-2105. https://doi.org/10.1177/1099636220909786

Giannopoulos, G.I., Kakavas, P.A. and Anifantis, N.K. (2008), "Evaluation of the effective mechanical properties of single walled carbon nanotubes using a spring based finite element approach", *Comput. Mater. Sci.* **41**(4), 561-569. https://doi.org/10.1016/j.commatsci.2007.05.016

Han, Y. and Elliott, J. (2007), Molecular dynamics simulations of the elastic properties of polymer/carbon nanotube composites. *Comput. Mater. Sci.* **39**(2), 315-323. https://doi.org/10.1016/j.commatsci.2006.06.011

Heidari, M. and Arvin, H. (2019), "Nonlinear free vibration analysis of functionally graded rotating composite Timoshenko beams reinforced by carbon nanotubes," *J. Vib. Control* **25**(14), 2063-2078. https://doi.org/10.1177/1077546319847836

Karamanlı, A. and Vo, T.C. (2021), "Finite element model for carbon nanotube-reinforced and graphene nanoplatelet-reinforced composite beams", *Compos. Struct.* 264. https://doi.org/10.1016/j.compstruct.2021.113739

Karami, B., Shahsavari, D. and Janghorban, M. (2018), "A comprehensive analytical study on functionally graded carbon nanotube-reinforced composite plates", *Aerosp. Sci. Technol.* **82-83**, 499-512. https://doi.org/10.1016/j.ast.2018.10.001

Khadir, A.I., Daikh, A.A. and Eltaher, M.A. (2021), "Novel four-unknowns quasi 3D theory for bending, buckling and free vibration of functionally graded carbon nanotubes reinforced composite laminated nanoplates", *Adv. Nano Res.*, **11**(6), 621-640. https://doi.org/10.12989/anr.2021.11.6.621

Khosravi, S., Arvin, H. and Kiani, Y. (2019a), "Interactive thermal and inertial buckling of rotating temperature-dependent FG-CNT reinforced composite beams", *Compos. B. Eng.* **175**, 107178. https://doi.org/10.1016/j.compositesb.2019.107178

Khosravi, S., Arvin, H. and Kiani, Y. (2019b), "Vibration analysis of rotating composite beams reinforced with carbon nanotubes in thermal environment", *Int. J. Mech. Sci.* **164**, 105187. https://doi.org/10.1016/j.ijmecsci.2019.105187

Kılıç, B. and Özdemir, Ö. (2021), "Vibration and stability analyses of functionally graded beams", *Arch. Mech. Eng.* **68**(1), 93-113. https://doi.org/10.24425/ame.2021.137043

Kiani, Y. and Eslami, M.R. (2013), "An exact solution for thermal buckling of annular FGM plates on an elastic medium", *Compos. B Eng.*, **45**(1), 101-110. https://doi.org/10.1016/j.compositesb.2012.09.034

Kollár, L.P. and Springer, G.S. (2003), *Mechanics of Composite Structures*, Cambridge University Press, U.K.

Lin, B., Chen, B., Zhu, B., Li, J., and Li, Y. (2021), "Dynamic stability analysis for rotating pre-twisted FG-CNTRC beams with geometric imperfections restrained by an elastic root in thermal environment", *Thin Wall. Struct.*, **164**, 107902. https://doi.org/10.1016/j.tws.2021.107902

Liu, Y., Wang, X., Liu, L., Wu, B. and Yang, Q. (2022), "On the forced vibration of high-order functionally graded nanotubes under the rotation via intelligent modeling", *Adv. Nano Res.* **13**(1), 47-61. https://doi.org/10.12989/anr.2022.13.1.047

Lu, X. and Hu, Z. (2012), "Mechanical property evaluation of single-walled carbon nanotubes by finite element modeling", *Compos. B. Eng.*, **43**(4), 1902-1913. https://doi.org/10.1016/j.compositesb.2012.02.002

Mangalasseri, A.S., Mahesh, V., Mukunda, S., Mahesh, V., Ponnusami, S.A., Harursampath, D. and Tounsi, A. (2023), "Vibration based energy harvesting performance of magneto-electro-elastic beams reinforced with carbon nanotubes", *Adv. Nano Res.*, **14**(1), 27-43. https://doi.org/10.12989/anr.2023.14.1.027

Mohamed, N., Mohamed, S.A. and Eltaher, M.A. (2020), "Buckling and post-buckling behaviors of higher order carbon nanotubes using energy-equivalent model", *Eng. Comput.*, **37**(4), 2823-2836. https://doi.org/10.1007/s00366-020-00976-2

Na, K.S. and Kim, J.H. (2004), "Three-dimensional thermal buckling analysis of functionally graded materials" *Compos. B: Eng.*, **35**(5), 429-437. https://doi.org/10.1016/j.compositesb.2003.11.013

Özdemir, Ő. (2016), "Application of the differential transform method to the free vibration analysis of functionally graded Timoshenko beams", *J. Theor. App. Mech.* **54**(4), 1205-1217. https://doi.org/10.15632/jtam-pl.54.4.1205

Özdemir Özgümüş, Ö. and Kaya, M.O. (2013), "Energy expressions and free vibration analysis of a rotating Timoshenko beam featuring bending–bending-torsion coupling", *Arch. Appl. Mech.*, **83**, 97-108. https://doi.org/10.1007/s00419-012-0634-4

Peng, X.L. and Li, X.F. (2010), "Thermal stress in rotating functionally graded hollow circular disks", *Compos. Struct.*, **92**(8), 1896-1904. https://doi.org/10.1016/j.compstruct.2010.01.008

Piovan, M.T. and Sampaio, R. (2009), "A study on the dynamics of rotating beams with functionally graded properties", *J. Sound Vib.*, **327**(1-2), 134-143. https://doi.org/10.1016/j.jsv.2009.06.015

Rahmani, B. (2018), "Adaptive fuzzy sliding mode control for vibration suppression of a rotating carbon nanotube-reinforced composite beam", *J. Vib. Control*, **24**(12), 2447-63. https://doi.org/10.1177/1077546316687937

Rayleigh, J.W.S.B (1877), *The Theory of Sound*, Dover Publications, New York, U.S.A.

Satankar, R.K., Sharma, N., Ramteke, P.M., Panda S.K. and Mahapatra, S.S. (2020), "Acoustic responses of natural fibre reinforced nanocomposite structure using multiphysics approach and experimental validation", *Adv. Nano Res.* **9**(4), 263-276. https://doi.org/10.12989/anr.2020.9.4.263

Shafiei, H. and Setoodeh, A.R. (2017), "Nonlinear free vibration and post-buckling of FG-CNTRC beams on nonlinear foundation", *Steel Compos. Struct.* **24**(1), 65-77. https://doi.org/10.12989/scs.2017.24.1.065

Shen, H.S.S. (2009), "Nonlinear bending of functionally graded carbon nanotube-reinforced composite plates in thermal environments", *Compos. Struct.* **91**(1), 9-19. https://doi.org/10.1016/j.compstruct.2009.04.026

Shen, H.S. and Xiang, Y. (2013), "Nonlinear analysis of nanotube-reinforced composite beams resting on elastic foundations in thermal environments", *Eng. Struct.*, **56**, 698-708. https://doi.org/10.1016/j.engstruct.2013.06.002

Shen, H.S. and Zhang, C.L. (2010), "Thermal buckling and postbuckling behavior of functionally graded carbon nanotube-reinforced composite plates", *Mater. Des.*, **31**(7), 3403-3411. https://doi.org/10.1016/j.matdes.2010.01.048

Shen, Z., Xia, J. and Cheng, P. (2019), "Geometrically nonlinear dynamic analysis of FG-CNTRC plates subjected to blast loads using the weak form quadrature element method", *Compos. Struct.*, **209**, 775-788. https://doi.org/10.1016/j.compstruct.2018.11.009

Sobhy, M. (2019), "Levy solution for bending response of FG carbon nanotube reinforced plates under uniform, linear, sinusoidal and exponential distributed loadings", *Eng. Struct.*, **182**, 198-212. https://doi.org/10.1016/j.engstruct.2018.12.071

Tian, J., Zhang, Z. and Hua, H. (2019), "Free vibration analysis of rotating functionally graded double-tapered beam including porosities", *Int. J. Mech. Sci.* **150**, 526-538. https://doi.org/10.1016/j.ijmecsci.2018.10.056

Torabi, J., Ansari, R., and Hassani, R. (2019), "Numerical study on the thermal buckling analysis of CNT-reinforced composite plates with different shapes based on the higher-order shear deformation theory", *Eur. J. Mech. A/Solids* **73**, 144-160. https://doi.org/10.1016/j.euromechsol.2018.07.009

Van Do, V.N., Jeon, J.T.T. and Lee, C.H.H. (2020), "Dynamic analysis of carbon nanotube reinforced composite plates by using Bézier extraction based isogeometric finite element combined with higher-order shear deformation theory", *Mech. Mater.*, **142**, 103307. https://doi.org/10.1016/j.mechmat.2019.103307

Vinyas, M. (2019), "A higher-order free vibration analysis of carbon nanotube-reinforced magneto-electro-elastic plates using finite element methods", *Compos. B. Eng.*, **158**, 286-301. https://doi.org/10.1016/j.compositesb.2018.09.086.

Wahrhaftig, A., Brasil, R.M.L.R.F. and Balthazar, J.M. (2013), "The first frequency of cantilevered bars with geometric effect: A mathematical and experimental evaluation", *J. Braz. Soc. Mech. Sci. Eng.* **35,** 457-467. https://doi.org/10.1007/s40430-013-0043-9

Wahrhaftig, A. de M. and Magalhães, K.M.M. (2021), "Bifurcation analysis of columns of composite materials with thermal variation", *Mater. Res.*, **24**. https://doi.org/10.1590/1980-5373-MR-2021-0266

Wang, C.Y. and Zhang, L.C. (2008), "A critical assessment of the elastic properties and effective wall thickness of single-walled carbon nanotubes", *Nanotechnology*, **19**(7), 75705. https://doi.org/10.1088/0957-4484/19/7/075705

Wattanasakulpong, N. and Ungbhakorn, V. (2013), "Analytical solutions for bending, buckling and vibration responses of carbon nanotube-reinforced composite beams resting on elastic foundation", *Compos. Mater. Sci.*, **71**, 201-208. https://doi.org/10.1016/j.commatsci.2013.01.028

Wu, Z., Zhang, Y. and Yao, G. (2020), "3/2 superharmonic resonance and 1/2 subharmonic resonance of functionally graded carbon nanotube reinforced composite beams", *Compos. Struct.* **241**, 112056. https://doi.org/10.1016/j.compstruct.2020.112056

Wu, Z., Zhang, Y., Yao, G. and Yang, Z. (2019), "Nonlinear primary and super-harmonic resonances of functionally graded carbon nanotube reinforced composite beams", *Int. J. Mech. Sci.* **153-154**, 321-340. https://doi.org/10.1016/j.ijmecsci.2019.06.039

Wu, H.L, Yang, J. and Kitipornchaj, S. (2016) "Nonlinear vibration of functionally graded carbon nanotube reinforced composite beams with geometric imperfections", *Compos. B Eng.*, **90**, 86-96. https://doi.org/10.1016/j.compositesb.2015.12.007

Wuite, J. and Adali, S. (2005), "Deflection and stress behaviour of nanocomposite reinforced beams using a multiscale analysis", *Compos. Struct.*, **71**, 388-396. https://doi.org/10.1016/j.compstruct.2005.09.011

Yas, M.H. and Samadi, N. (2012), "Free vibrations and buckling analysis of carbon nanotube-reinforced composite Timoshenko beams on elastic foundation", *Int. J. Press. Vessels Pip.* **98**, 119-128. https://doi.org/10.1016/j.ijpvp.2012.07.012

Zhang, D.G. (2014) "Thermal post-buckling and nonlinear vibration analysis of FGM beams based on physical neutral surface and high order shear deformation theory", *Meccanica*, **49**(2), 283-293. doi:10.1007/s11012-013-9793-9

Zhang, L.W., Song, Z.G. and Liew, K.M. (2015), "State-space Levy method for vibration analysis of FG-CNT composite plates subjected to in-plane loads based on higher-order shear

deformation theory", *Compos. Struct.*, **134**, 989-1003. https://doi.org/10.1016/j.compstruct.2015.08.138
Zhou, T. and Song, Y. (2019), "Three-dimensional nonlinear bending analysis of FG-CNTs reinforced composite plates using the element-free Galerkin method based on the S-R decomposition theorem", *Compos. Struct.*, **207**, 519-530. https://doi.org/10.1016/j.compstruct.2018.09.026
Zhu, P., Lei, Z.X. and Liew, K.M. (2012), "Static and free vibration analyses of carbon nanotube-reinforced composite plates using finite element method with first order shear deformation plate theory, *Compos. Struct.*, **94**(4), 1450-1460. https://doi.org/10.1016/j.compstruct.2011.11.010

CC

Nomenclature

CC: Clamped-clamped end conditions
CF: Clamped-free end conditions
CH: Clamped-hinged end conditions
CNTs: Carbon nanotubes
CNTRCs: Carbon-nanotube-reinforced composites
FEM: Finite element method
FGCNTRC: Functionally graded carbon-nanotube-reinforced composite
FGMs: Functionally graded materials
HH: Hinged-hinged end conditions
PMMA: Polymethyl methacrylate
SWCNTs: Single-walled carbon nanotubes
TBT: Timoshenko beam theory
A: Cross-sectional area of beam
b: Width of the beam
C_1, C_2: Integration constants
E_{11}, E_{22}: Direction-dependent effective Young's moduli of CNTRC (MPa)
E_{11}^{CNT}, E_{22}^{CNT}: Direction-dependent Young's moduli of CNTs
E_m: Young's modulus for the isotropic matrix material
EA: Axial stiffness
F_{CF}: Centrifugal force
G_{12}: Effective shear modulus of CNTRC
G_{12}^{CNT}: Shear modulus of CNTs
G_m: Shear modulus of the isotropic matrix material
h: Height of the beam
I_1, I_2: Inertial characteristics
K: Kinetic energy
k: Shear correction factor
L: Length of the beam
L_i: Offset of each element from the rotational axis
M_T: Thermal moment
M_x: Mechanical bending moment
$\overline{N_{cr}}$: Dimensionless critical buckling load
N_e: Number of elements
N_T: Thermal axial force
N_x: Mechanical axial force
P_0: Reference point before deformation
P: Reference point after deformation
P_{cr}: Critical buckling load
$\overline{P_i}(i = 0, \dots, 4)$: Coefficients of the interpolation function
Q: Shear force
R: Beam radial distance
T: Ambient temperature
T_0: Initial temperature
T_b: Temperature of the bottom surface
T_t: Temperature of the top surface
u_0: Axial displacement
U: Potential energy
$\vec{V}$: Velocity vector
V_{cnt}^* : Volume fraction of CNT
V_m : Volume fraction of matrix
V_x, V_y, V_z: Velocity components
W_{CNT} : CNT mass fraction
w : Flapwise bending deflections
$[K^e]$: Element stiffness matrix
$[K^e]_f$: Element flexural stiffness matrix
$[K^e]_g$: Element geometric stiffness matrix
$[K^e]_s$: Element shear stiffness matrix
$[M^e]$: Element mass matrix
x, y, z : Global coordinate system
x', y', z': Local coordinates
$\bar{z}_0$: Physical neutral surface of the FGCNT-reinforced beam
α_{11}: Effective specific heat coefficient
α_{CNT}: Specific heat coefficient of carbon nanotubes
α_M: Specific heat coefficient of matrix material
$\gamma_{x\mu}$, $\gamma_{x\xi}$: Shear strains
ΔT: Temperature difference
δ: Dimensionless hub radius
ε_0: Uniform strain
ε_T: Thermal strain
ε_{xx}: Axial strain
η_i: Efficiency constants (η_1, η_2, η_3)
θ: Rotation angle due to flapwise bending
κ: Thermal conductivity coefficient
μ: Local cross-sectional location
ξ: Local cross-sectional location
ρ: Density of the beam
ρ_{CNT} : Density of CNTs
ρ_m : Density of matrix
σ_{xx}: Normal stress
$\tau_{x\xi}$: Shear stress
υ: Poisson's ratio
υ_{12}, υ_{21}: Effective Poisson's ratio
υ_{12}^{CNT}, υ_{21}^{CNT}: Poisson's ratio for carbon nanotube
υ_m: Poisson's ratio for matrix
φ: Rotation angle due to bending
$\bar{\omega}$: Dimensionless natural frequency
Ω: Angular speed of the rotating beam (rad/s)
$\bar{\Omega}$: Dimensionless rotational speed